Characterization of sprayed deposited $(SnS_2)_X (CdS)_{1-X}$ composite thin films

M. N. AMROUN, M. KHADRAOUI*, R. MILOUA, N. BENRAMDANE, K. SAHRAOUI, Z. KEBBAB
Laboratoire d'Elaboration et de Caractérisation des Matériaux, département d'électronique, Université Djillali Liabes, BP89, Sidi Bel Abbés 22000, Algeria

$(SnS_2)_x (CdS)_{1-x}$ composite thin films have been prepared for the first time by the spray pyrolysis method on glass substrates using Tin chloride ($SnCl_2$-$2H_2O$) and Cadmium chloride ($CdCl_2$) as precursors. The films were characterized by X-Ray diffraction (XRD), Scanning Electron Microscopic (SEM), optical absorption and electrical resistivity measurement techniques. With the structural investigations, SnS_2, CdS thin films and SnS_2–CdS composite thin films formation was confirmed. Optical properties of the deposited films were obtained using transmittance measurements in the wavelength range [200–2500 nm]. The optical band gaps for the films with variable composition (x= 1, x = 0.8, x=0.6 and x = 0) are found to lie between those of the SnS_2 and CdS ones. The electrical conductivities were measured in the temperature range 300-395 K. The resistivity and activation energy are found x dependent.

(Received April 6, 2016; accepted November 28, 2017)

Keywords: SnS_2, CdS, Thin films, Spray Pyrolysis

1. Introduction

The semi-conducting thin films especially nanocrystalline have been playing an important role in the development of solar selective coatings, solar cells, photoconductors, antireflection coatings, wave guide coatings IR detectors, photo thermal solar coatings etc.[1].

Recently, various techniques and methods have been applied to deposit n-type chalcogenide binary and ternary thin films. Cadmium sulfide (CdS) is a wide gap semiconductor (Eg= 2.40 eV), widely used in many fields of science and technology due to its interesting chemical and physical properties. In particular is an interesting material for applications in optoelectronic, integrated optics and photovoltaic devices. CdS thin films were prepared by various methods such as sputtering [2], electrochemical deposition [3],vacuum deposition [4] and spray pyrolysis deposition [5]. Among all the techniques, spray pyrolysis appears to be the best technique to deposit CdS thin films with suitable properties for various device applications due to its simplicity and low cost.

Tin disulfide adopts the PbI2 layered structure with hexagonal unit cell, in which tin atoms are located in the octahedral sites between two hexagonally close packed sulfur slabs to form a sandwich structure. SnS_2 has interesting properties such as high optical absorption coefficient ($>10^4$ cm^{-1}) in the visible range, wide optical band gap of about 2,12-2.44eV, n-type electrical conduction and high photo-conducting behavior [6,7,8]. These properties suggest that SnS_2 is an appropriate material for solar cell and opto-electronic device applications [9]. In the present work, a spray pyrolysis method was used to fabricate $(SnS_2)_x(CdS)_{1-x}$ thin films with composition (x= 1, 0.8, 0.6 and 0) .

In recent years the composite thin films such as $(CdS)_X (PbS)_{1-X}$ [10], $CdS–Cu_X S$ [11], $Cd_{1-X} Sn_X S$ [12], $(Sn_2S_3)_x (Bi_2S_3)_{1-x}$ [13], $Cd_{1-X} Zn_X S$ [14] have attracted attention for their possible application in photovoltaic devices fabrication due to the modification in electrical and optical properties.

To the best of our knowledge, there is no published report on the composite semiconductor thin film based on CdS and SnS_2 using a low cost process such as spray pyrolysis. The main aim is to exploit the different properties of CdS and those of SnS_2 in thin films to increase the yield in the photovoltaic cells

2. Experimental

$(SnS_2)_x (CdS)_{1-x}$ thin films were deposited by the spray pyrolysis technique [15,16], using tin chloride($SnCl_2$,$2H_2O$) and thiouréa $CS(NH2)_2$ on microscope glasses of $(75*25)mm^2$. The molarity of the prepared solution is 0.1 M. The $SnCl_2$ was dissolved in a mixture of methanol and deionised water in the ratio of 1:1, a few drops of HCl were also added for complete dissolutions to the solubility of $SnCl_2$, while the thiourea was dissolved in deionised water. The prepared solutions of tin chloride and thiourea were appropriately mixed to obtain an Sn:S proportion of 1:1. For the preparation of CdS, we followed the same procedure as before except that in this case the CdCl2-$2H_2O$ powder was used instead of $SnCl_2$-$2H_2O$ and dissolved in deionised water only. The solutions obtained were pulverised on glass substrates with compressed air (2 bars) at a flow rate of 8 ml/min. The substrate temperature was maintained at 350°C. The distance from the spray nozzle to the heater was kept at

approximately at 29 cm. Under these deposit conditions, good films are obtained. They are uniform and very adherent to the substrates.

In this paper we have described the preparation of mixed $(SnS_2)_x (CdS)_{1-x}$ by the spray pyrolysis method with variable composition (x=1, 0.8, 0.6 and 0). Structural characterisation has been carried out at room temperature using a Philips 1830 X-ray diffractometer with a Cu Kα peak λ=1.546Å. The optical transmittance was recorded from 200 to 2500 nm wavelength using an UV (Ultra-Violet) Visible JASCO type V-570 double beam spectrophotometer. The electrical properties were measured by ECOPIA HMS-5000 Hall Effect measurement at room temperature, and by the four-point probe method. Morphology was carried out by a Joel JSM 5800 scanning electron microscope.

3. Results and discussion

3.1. Structural characterization

Thin films of $(SnS_2)_x (CdS)_{1-x}$ were characterized through XRD measurements in order to obtain information regarding the phase, crystalline structure and lattice parameters…the values are given in Table 1. The XRD patterns of composite thin films $(SnS_2)_x (CdS)_{1-x}$ with variable composition x = 0, 0.8, 0.6 and 1, deposited at 350°C by spray pyrolysis technique were shown in Fig. 1. The peaks of XRD pattern have been assigned in accordance with the JCPDS cards of SnS_2 (Card No. 23-0677) and CdS (Card No 41-1049). For x=0, all the peaks can be indexed to the phase of CdS, and for x=1, all the peaks are attributed to the phase of SnS_2 with the dominant peak (0 0 1) reflection, at x=0.8 and x=0.6, the XRD patterns clearly demonstrate three well defined peaks for CdS (2θ=24.98, 2θ=26.68, 2θ=28.36) and one peak for SnS_2 (2θ=14.95), The XRD results of deposited films reveal the presence of the both hexagonal phases. These observations confirm the formation of composites films and the coexistence of two separate phases (CdS and SnS_2).These films were not treated after deposition.

The structural parameters such as; lattice constants (a and c), crystallite size (G), dislocation density (δ) and micro-strain (ε) were calculated from XRD data and listed in Table 1. All the peaks can be indexed to hexagonal structure. In the case of hexagonal system, to evaluate the lattice parameters using the following expression [16]:

$$d_{hkl} = \frac{a}{\sqrt{\frac{4}{3}(h^2+k^2+hk)+l^2\frac{a^2}{c^2}}} \qquad (1)$$

where (h,k,l) are Miller indices of refractor planes appearing on the diffraction spectrum and d_{hkl} their inter-reticular distances. Applying this relation to the most intense peaks provided by diffraction spectra, to determine the lattice parameters « a ›› and « c ›› of the structure , It is observed the lattice constants 'a' and 'c' values are in good agreement with JCPDS cards mentioned previously, It is observed that (Table 1). The variation in c_{SnS2} is situated between 5.921 Å and 6.041 Å (Δc_{SnS2}=0.12 Å) which is greater than the variation in c_{CdS} and a_{CdS}.

This can be related to the difference of 0.04 Å in ionic radius of (r_{Cd++} = 0.97 Å and r_{Sn++} = 0.93Å).

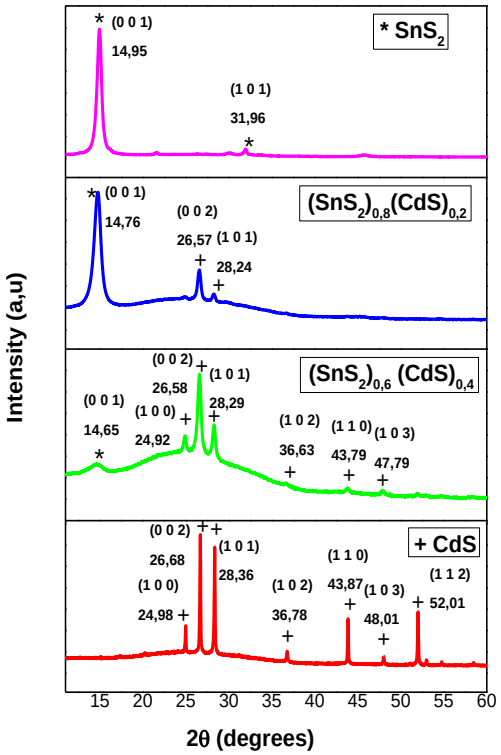

Fig. 1. Experimental X-ray diffraction pattern of the Composite $(SnS_2)_x (CdS)_{1-x}$ prepared by the spray pyrolysis method

The grain size (G) of the deposited films was calculated by using Scherrer's formula [16, 17]:

$$G = \frac{k.\lambda}{\beta.\cos\theta} \qquad (2)$$

where k= 0,9 is the shape factor, **λ** is the X-ray wavelength in Å, θ is the Bragg angle, and β is defined as the full width at half maximum (FWHM) of the most intense diffraction peak (001) for the SnS_2 and (002) for the CdS. In Fig. 2 the variation of grain size of $(SnS_2)_x (CdS)_{1-x}$ composite thin films as a function of composition x is shown, The value of grain size of CdS are found to be in excellent agreement with those reported by S.Aksay et al [18]. The grain size of (002) peak CdS decreases from 88.26 nm to 19.85nm as 'x' changes from 0 to 0.6 but then increases to 22.76 nm for x = 0.8.

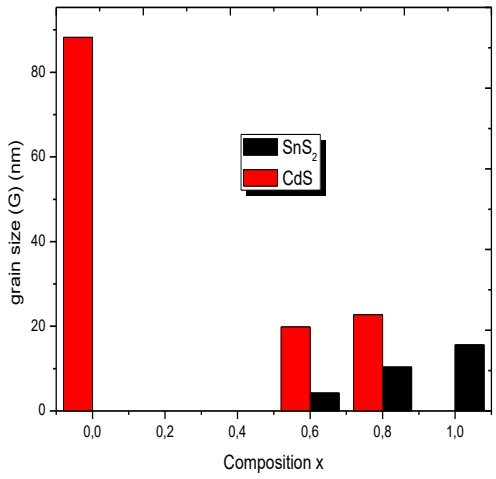

Fig. 2. Variation of grain size G as function of concentration x

The origin of the strain is related to the lattice misfit which in turn depends upon the deposition conditions. The micro-strain (ε) developed in the thin film is calculated from the following relation

$$\varepsilon = \frac{\beta \cdot \cos\theta}{4} \quad (3)$$

However, the dislocation density (δ), defined as the length of dislocation lines per unit volume of the crystal, was estimated by using relation [19].

$$\delta = \frac{1}{D^2} \quad (4)$$

The calculate values of the grain size (G), strain (ε) and dislocation density (δ) are listed in Table 1.

It is observed the small dislocation and micro-strain of the films and the corresponding values are recorded for (002) peak CdS film. For (001) peak SnS_2, it is observed that the micro-strain and dislocation density increase with increasing CdS concentration. The dislocation density of $(SnS_2)_x$ $(CdS)_{1-x}$ is 41.14 10^{10} and 1.28 10^{10} lines/cm^2 at x=1 and 0 respectively. The smallest value of (ε) was calculated as much as 4.37 10^{-4} for x=0 and the greater value as much as 91.26 10^{-4} for x=0.6 the (001) peak SnS_2.

One can observe that there is an inverse relationship between the grain size and dislocation density. This explains that the dislocation density contributes to the smash grain. It is noted that the micro-strain have an inverse variation to that of the grain size. This variation in strain and dislocation density may influence the properties of nanostructured thin films.

Increasing Sn concentration could degrade the crystallinity of the composite films due to small crystallites in the films. The decrease of grains size of the CdS films with increasing Tin content it is also observed by Tulay Ozer et al [12].

3.2. Surface morphology

Surface morphology of material plays an important role in fabrication of solar energy devices, Scanning electron microscopy (SEM) photographs are used for studying the surface morphology of the films. Fig. 3 illustrates the surface morphology of the composite $(SnS2)_x$ $(CdS)_{1-x}$ (x=1, 0.8, 0.6 and 0) thin films on glass substrates by Spray pyrolysis methods. It is observed that the films are continuous over the glass surface.

There are no macroscopic defects such as voids, peeling or cracks. Fig. 3(a) show SnS_2 film, the surface of the film is highly smooth comprising small spherical grains. it is clearly seen that the particles forming the films are in nano scale.

Table 1. The structural characterization of Composite $(SnS_2)_x$ $(CdS)_{1-x}$ thin films

Concentration (x)	Phase	(h k l) Crystal system	Lattice constants (A°)		The grain size (G) (nm)	Dislocation density (δ) (10^{10} lines/cm^2)	Strain (ε) (10^{-4})
			a	c			
x= 1	SnS_2	(001)	3.666	5.921	15.59	41.14	24.78
x = 0.8	$(SnS_2)_{0.8}(CdS)_{0.2}$	(001)	3.663	5.996	10.39	92.63	37.19
		(002)	4.132	6.704	22.76	19.30	16.97
x = 0.6	$(SnS_2)_{0.6}$ $(CdS)_{0.4}$	(001)	3.641	6.041	4.23	558.88	91.26
		(002)	4.124	6.701	19.85	25.37	19.46
x = 0	CdS	(002)	4.115	6.677	88.26	1.28	4.37

For x =0.6 i.e. for $(SnS2)_{0.6}$ $(CdS)_{0.4}$, the distribution of the particles is non-homogeneous, both smooth surface and larger grains observed at some places. Thus it is seen that, addition of CdS in SnS_2 increases the grain size of the films composite. It is clear that surface morphology of as deposited $(SnS2)_{0.8}$ $(CdS)_{0.2}$ composite is totally different

with those of CdS and SnS_2 thin films. It is observed that the as-deposited $(SnS2)_{0.8}(CdS)_{0.2}$ the film surface is composed of multicornered and nanocrystalline grains are formed by agglomeration of small particles having irregular shapes grains, and we can see that the film covers the entire glass substrate. The crystallinity of the film improves and the grain size of the composite film becomes large with incorporation of the cadmium in the solution.SEM images thus reveals that the grain size of the composite films is generally smaller than that of the pure CdS thin films, and bigger than that of pure SnS_2. These results are consistent with that obtained from the Fig 2. For CdS film (x=0). SEM shows film is continuous with continuous distribution of well-covered grains. It can be seen as the films exhibits coarse grains with high surface roughness.

3.3. Optical characterization

The optical properties of $(SnS_2)_x$ $(CdS)_{1-x}$ were determined from the optical transmittance T at room temperature with unpolarized light at normal incidence. The measurements were recorded in the range 200_2500 nm using a JASCO V-570 spectrophotometer.

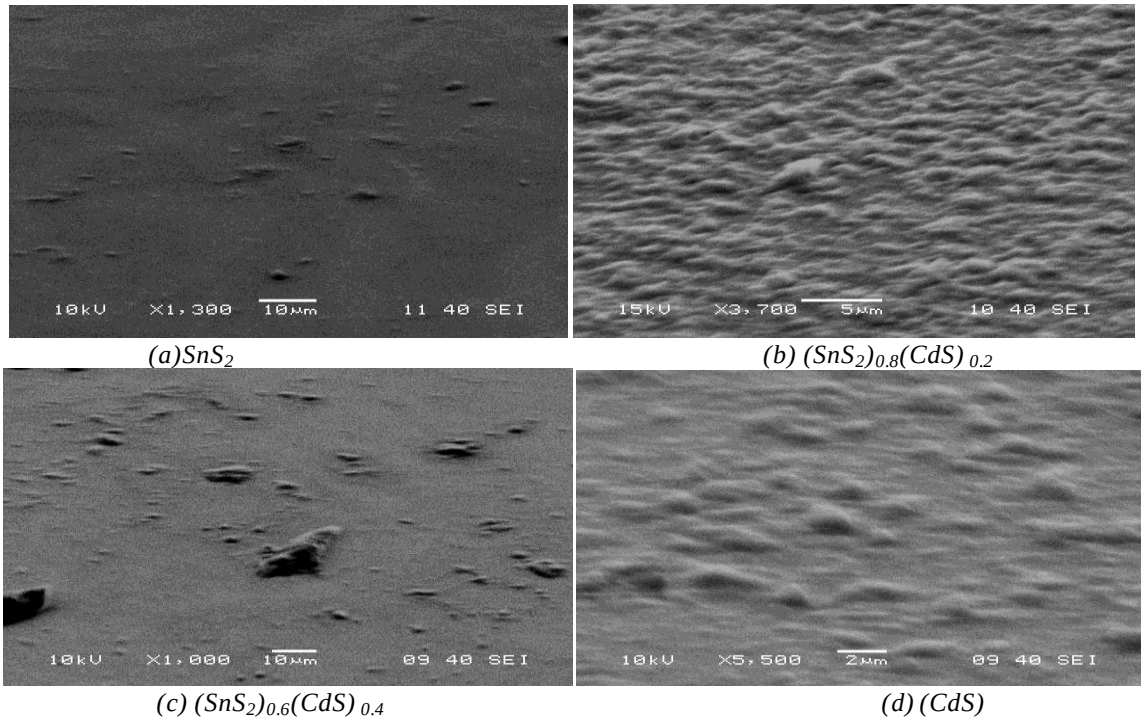

(a)SnS_2 *(b) $(SnS_2)_{0.8}(CdS)_{0.2}$*

(c) $(SnS_2)_{0.6}(CdS)_{0.4}$ *(d) (CdS)*

Fig. 3. SEM images of $(SnS_2)_x$ $(CdS)_{1-x}$ thin films with different concentrations x=1, 0.8, 0.6 and 0.

Fig. 4 shows the optical transmittance curves as a function of wavelength for the composite $(SnS_2)_x$ $(CdS)_{1-x}$ thin films.

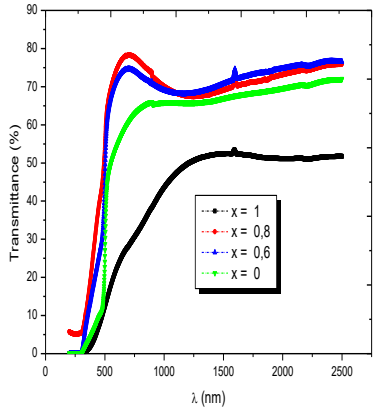

Fig. 4. Optical transmittance of the composite $(SnS_2)_x$ $(CdS)_{1-x}$ thin films

The films present an absorption edge of approx. 500 nm. The average transmittance of the films varies between 50–79 %. The highest transmittance obtained was 79 % for x=0.8 and the lowest was 35% for SnS_2 (x=1) film both on the visible region (500_850nm). In the optical transmittance spectra (Fig 4) will appear a shoulder. We suggest that this is interference and not the presence of the absorption edges. Also by this result, we show the formation of $(SnS_2)_x$ $(CdS)_{1-x}$ composites and the existence of one gap

In order to find the band gap (Eg) values of the films, initially the absorption coefficient (α) should be identified by the following relation:

$$\alpha = \frac{1}{d}\ln\left(\frac{1}{T}\right) \quad (5)$$

where, d is the film thickness. The variation of the absorption coefficient (α) of $(SnS_2)_x$ $(CdS)_{1-x}$ films is shown in Fig. 5 as a function of wavelength. The evaluated

optical absorption coefficient of the films was upper 10^{+4} cm^{-1}.

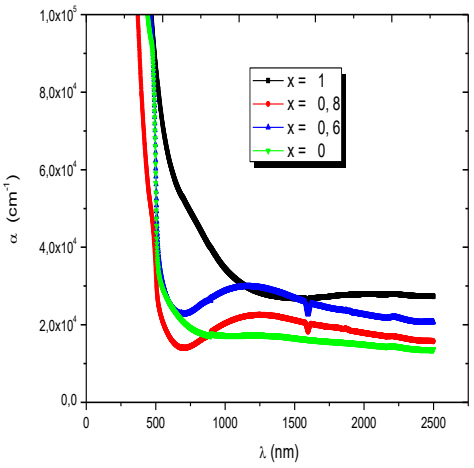

Fig. 5. Optical absorption vs. wavelength (nm) of the composite $(SnS_2)_x$ $(CdS)_{1-x}$ thin films

The optical band gap of the films is formally defined as the intercept of the plot $(\alpha h\upsilon)^2$ as a function of photon energy hυ, using the relation [20].

$$(\alpha hv)^m = An.(hv - E_g) \quad (6)$$

where m=2 is for a direct allowed transition and m=1/2 is for an indirect allowed transition and An is a constant.

The energies band gap of the thin films $(SnS_2)_x(CdS)_{1-x}$ was estimated by extrapolating the linear part of the $(\alpha h\upsilon)^2$ against hυ plot the horizontal axis, as shown in Fig. 6. The values (Eg) corresponding to the direct band-gap transition of the $(SnS_2)_x$ $(CdS)_{1-x}$ thin films are listed in Table 2, It is found that the band gaps of composite films $(SnS_2)_x$ $(CdS)_{1-x}$ lie in between individual band gaps of SnS_2 and CdS. The value (Eg) corresponding to the direct band-gap transition of the SnS_2 and CdS thin films was found to be 2ev and 2.4ev respectively, these results are in good agreement with the value obtained by O.A.Yassin et al. [21] and by S. Aksay, M. Polat et al.[18.22] respectively. For x=0.6 films, the estimation of the band gap value is identical and equal to 2.40 (±0.01) eV this suggests that the introduction of Sn does not very affect the band gap of the CdS films [12].

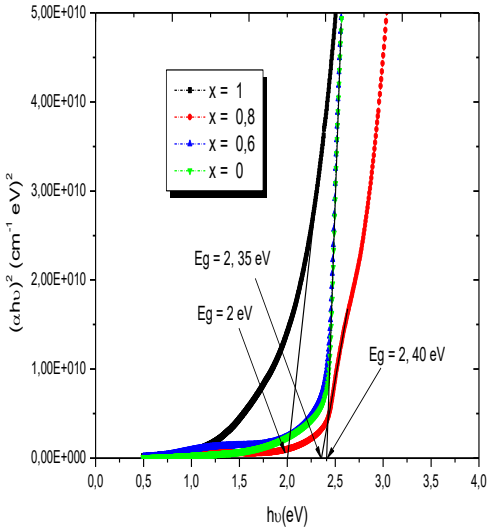

Fig. 6. Plot of $(\alpha h\upsilon)^2$ versus hυ for the composite $(SnS_2)_x$ $(CdS)_{1-x}$ thin films

The absorption coefficient of the thin films sample shows a tail for sub-band gap photon energy. The Urbach energy E_{00} associated to the width of the tail can be measured from the fit of data to [23].

$$\alpha = \alpha_0 \exp(h\upsilon / E_{00}) \quad (7)$$

where α_0 is a constant and E_{00} is the band tail width, which represents the degree of disorder [24].

The value of E_{00} is determined from the reciprocal of the slope of the relation between ln α and hv, and the value of E_{00} is given in Table 2.

Table 2. Thickness, Band gap energy and Urbach energy of $(SnS_2)_x$ $(CdS)_{1-x}$.thin films

Composition x	Film composition	Band gap energy(eV)	Urbach energy E_{00} (eV)	Thickness (d) (nm)
x=1	SnS_2	2	0.79	240
x=0.8	$(SnS_2)_{0.8}$ $(CdS)_{0.2}$	2.35	0.25	174.74
x=0.6	$(SnS_2)_{0.6}$ $(CdS)_{0.4}$	2.4	0.16	128.97
x=0	CdS	2.4	0.137	240.95

In Fig. 7 we have reported the variation of the optical gap together with the band tail width as a function of the composition x. for x =1 the Urbach energies have the highest values which is an indication of a large structural disorder. As can be seen, the optical gap variation with the x composition is opposite to the disorder variation, this suggests that the optical gap is controlled by the disorder in the film network.

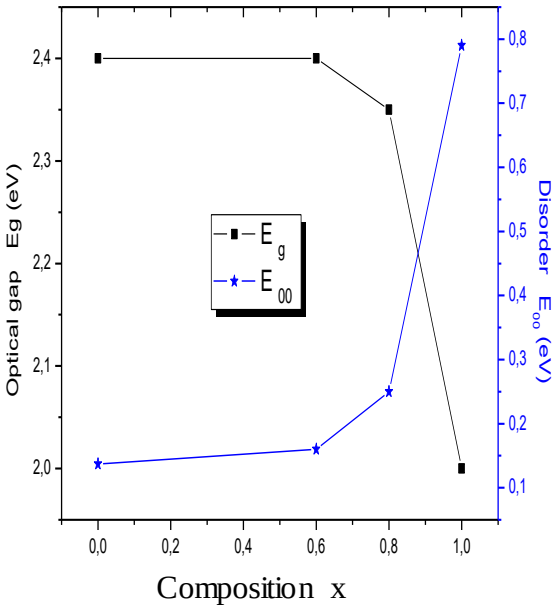

Fig. 7. Optical gap and Urbach's energy of $(SnS_2)_x (CdS)_{1-x}$ vs the composition x

3.4. Electrical characterization

The temperature dependence electrical resistivity of spray deposited $(SnS_2)_x (CdS)_{1-x}$ thin films was studied using a four-point probe method in the temperature range of 300-395 K. It is observed that conductivity increases with increase in the temperature, which shows that all the films are semiconducting and non-linear nature of the plots show the presence of many defect levels in the films.

The activation energy (E_a) was determined by The Arrhenius equation:

$$\sigma = \sigma_0 \exp\left(\frac{-E_a}{KT}\right) \quad (8)$$

Where σ is the conductivity, σ_0 is a constant, K the Boltzmann constant, T the Temperature. The curve of log (σ) versus 1000/ T (k^{-1}) was showed in fig.8.through the slope of the fitted line we can estimate E_a for the films, the calculated values of E_a are given in Table3. The activation energy is calculated, which is 0.04 eV for SnS_2 film and it increases with cadmium addition and becomes 0.109 eV for CdS. The activation energy of the as deposited composite film $(SnS_2)_x (CdS)_{1-x}$ is in between that of the SnS_2 and CdS.

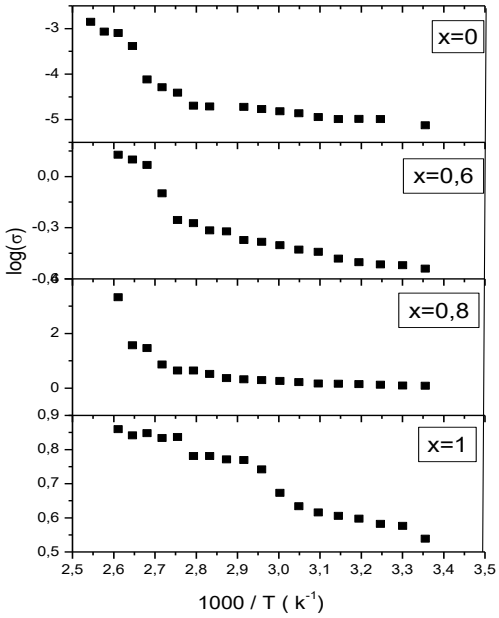

Fig. 8. Plots of log (σ) vs 1000/ T (k^{-1}) for the $(SnS_2)_x (CdS)_{1-x}$ thin films

Table 3. Activation energy and The Hall Effect results of films compositions

Films	Resistivity ρ(Ωcm)	Mobility (cm^2/Vs)	Bulk concentration (cm^{-3})	Hall coefficient (cm^3/C)	Sheet Resistance Rsh (Ω)	Activation energy E_a (ev)
SnS_2	$2.74\ 10^{-2}$	$4.54\ 10^{+1}$	$-5.00\ 10^{+18}$	-1.24	$1.14\ 10^{+3}$	0.04
$(SnS_2)_{0.8}(CdS)_{0.2}$	$5.24\ 10^{-2}$	$2.64\ 10^{-1}$	$-4.50\ 10^{+20}$	$-1.38\ 10^{-2}$	$3.01\ 10^{+3}$	0.056
$(SnS_2)_{0.6}(CdS)_{0.4}$	$3.32\ 10^{-2}$	1.12	$-1.67\ 10^{+20}$	$-3.73\ 10^{-2}$	$2.60\ 10^{+3}$	0.041
CdS	$2.22\ 10^{+4}$	$6.51\ 10^{+1}$	$-1.26\ 10^{+12}$	$-4.92\ 10^{+6}$	$5.98\ 10^{+6}$	0.109

The Hall Effect measurements of the composite thin films $(SnS_2)_x (CdS)_{1-x}$ have been studied at room temperature. Electrical resistivity, mobility, Bulk concentration and Hall coefficient are given in Table 3. The negative sign of hall coefficient confirms n-type conductivity of the films. The electrical resistivity of composite thin films is between SnS_2 and CdS. one can observe that for pure CdS, strong value of resistivity is seen ($2.22\ 10^{+4}$ Ω cm). This value starts to decrease rapidly when the concentration of Tin in the precursor solution increased ($3.32\ 10^{-2}$ Ω cm for x=0.6). The minimum resistivity of the composite films has been observed for SnS_2 ($2.74\ 10^{-2}$ Ω cm).

The carrier concentrations of the CdS film is in the order of (-1.26 10^{+12} cm^{-3}) which is in good agreement with that of chemical pyrolysis deposited CdS films [25]. The increase of Tin concentration causes an increase in carrier concentration at x = 0.8 and x = 0.6.

The increase in the carrier concentrations can be explained by the substitution of Sn^{2+} ions at the Cd^{2+}sites leading to decrease of the resistivity. As the doping level increased, more dopant atoms occupy the cadmium lattice sites, which results in more charge carriers. Also the large concentration of free electrons measured in $(SnS_2)_{0.8}(CdS)_{0.2}$ and $(SnS_2)_{0.6}(CdS)_{0.4}$ films by comparison to CdS and SnS_2 ones .might be attributed to the less structural disorder (low value of Urbach Energy) (see Table 2).

4. Conclusions

A simple and convenient spray pyrolysis method can be employed to deposit good quality $(SnS_2)_x$ $(CdS)_{1-x}$ composite thin films. The deposited films are uniform and adherent to the substrate. The electrical, optical and structural properties of composite $(SnS_2)_x$ $(CdS)_{1-x}$ thin films were studied. The XRD studies revealed that $(SnS_2)_x$ $(CdS)_{1-x}$ thin films are_hexagonal structure and confirmed mixed phases of the composite thin films for x=0.8 and 0.6. The optical properties showed that band gap energy changes from 2eV to 2.4eV depending on film composition, SEM studies reveal that as deposited composite material is of nanodimensions and have a mixed phase of CdS (hexagonal) and SnS_2 (hexagonal).These properties can be well used in solar energy conversion devices.

References

[1] H. M. Pathan, C. D. Lokhande, Bull. Mater. Sci. **27,** 85 (2004).
[2] M. A. Islam, et al., Energy Procedia **33**, 203 (2013).
[3] U. Demir, C. Shannon, Langmuir **10**(8), 2794 (1994).
[4] N. A. Shah, et al., J. Alloys Compd. **512**(1), 185 (2012).
[5] S. J. Ikhmayies, R. N. A. Bitar, Appl. Surf. Sci. **256,** 3541 (2010).
[6] B. Thangaraju, P. Kaliannan, J. Appl. Phys. **33,** 1054 (2000).
[7] G. Said, P. A. Lee, Phys. Status Solidi A Appl. Res. **15**, 99 (1973).
[8] G. Domingo, R. S. Itoga, C. R. Kannewurf, Phys. Rev. **143,** 356 (1966).
[9] T. Jiang, G. A. O. Ozine, A. Verma, R. L. Bedard, J. Mater. Chem. **8,** 1649 (1998).
[10] L. P. Deshmukh, B. M. More, S. G. Holikatti, P. P. Hankare, Bull. Mater. Sci. **17,** 555 (1994).
[11] P. K. Nair, M. T. S. Nair, J. Compos, Proc. SPIE **823,** 256 (1987).
[12] T. Özer, S. Kose, Int. J. Hydrogen Energy **34,** 5186 (2009).
[13] M. Khadraoui, R. Miloua, N. Benramdane, A. Bouzidi, K. Sahraoui, Materials Chemistry and Physics **169**, 40 (2015).
[14] L. P. Deshmukh, C. B. Rotti, K. M. Garadkar, G. S. Sahane, Ind. J. Pure Appl. Phys. **36**, 322 (1998).
[15] M. Khadraoui, N. Benramdane R. Miloua, C. Mathieu, A. Bouzidi, K. Sahraoui, Optoelectron. Adv. Mat. **9**(9-10), 1167 (2015).
[16] M.N. Amroun, M. Khadraoui, R. Miloua, Z. Kebbab, K. Sahraoui, Optik **131**, 152 (2017).
[17] B. E. Warren, X-ray Diffraction, 2nd ed., Dover, New York, 1990, pp. 1.
[18] S. Aksay, M. Polat, T. Ozer, S. Kose, G. Gurbuz, Applied Surface Science **257,** 10072 (2011).
[19] G. B. Williamson, R. C. Smallman, Philos. Mag. **1,** 34 (1956).
[20] P. Kireev, La Physique Des Semiconducteurs, Mir, Moscou, 1975
[21] O. A. Yassin, A. A. Abdelaziz, A. Y. Jaber, Materials Science in Semiconductor Processing **38,** 81 (2015).
[22] S. Sze, Physic of semiconductor devices, John Wiley & Son, New York, 1981.
[23] M. V. Kurik, Phys. Status Solidi A **8,** 9 (1971).
[24] J. Olley, Solid State Commun. **13,** 1437 (1973).
[25] D. Cha, S. Kim, N. K. Huang, Mater. Sci. Eng. B: Solid State Mater. Adv.Technol. **106**, 63 (2004).

*Corresponding author: khadraoui_hm@yahoo.fr